Manufacturability of composite laminates with integrated thin film Li-ion batteries

Federico Gasco and Paolo Feraboli

Abstract

The limits of processability of solid-state thin film lithium-ion batteries embedded into composite laminates are identified through testing under pressure, temperature and a liquid resin environment representative of composite processing cycles. Battery failures are characterized based on optical microscopy and capacity retention, and three distinct types of failures are recognized and analyzed. Failures are associated either with the battery polymeric sealant failure or with the physiochemical degradation of the electrolyte or the anode. Results give evidence that the cure temperature is the most influential parameter for battery survivability. Based on these experimental results, the optimum curing cycle is identified and embedding tests that retain full battery capacity are successfully performed. The minimal three-layer battery packaging proves to be an efficient air and moisture barrier within the above conditions.

Keywords

Multifunctional structures, energy harvesting, energy storage, smart structures

Introduction

The flight endurance of an electric propeller-driven unmanned aerial vehicle (UAV) is significantly improved by reducing the weight more so than increasing the battery capacity.[1] Moreover, the structure and the battery each typically contribute 20–40% to the total UAV mass.[1,2] The consolidation of battery and structure can theoretically reduce the total weight by exploiting the battery components as load-bearing elements and by eliminating battery fittings or supports. In addition, rather than bulky, centralized batteries, the integration of multiple lightweight batteries into the structure enables distributed power supply and storage, potentially reducing the amount of wiring.

However, to date, system performance improvements achieved with such integration have been documented only for applications demanding low mechanical stress.[3] Furthermore, the current battery technology, based on microstructured lithium (Li) intercalation compounds, is such that high specific energy and specific power, as well as good mechanical properties cannot be achieved.[3–8] In order to meet the requirements for the next generation of airborne, load-bearing batteries, solid-state thin film Li-ion batteries (TFBs) have been recently proposed.[9–13] The thin film structure maximizes the specific contact surface between electrodes and electrolyte, thereby increasing the electric stored energy and power per unit mass by increasing the fraction of reactants and the rate of the electrochemical reaction, respectively. Downsizing the electrodes and electrolyte to a thin film dramatically reduces the path length for ionic and electronic transport, allowing to achieve the desired conductivity without utilizing conventional porous compounds comprising electrically conductive lattices and binders, leading to higher energy and power density. Moreover, scalable manufacturing processes for nanostructured materials, such as electrospinning, chemical vapor deposition (CVD) and atomic layer deposition (ALD), are suitable for TFB manufacturing. The future application of nano-scale technology to the battery active components can potentially lead to several advantages. First, it allows further increase of TFB capacity and power by decreasing the path length of Li-ion and electronic transportation.[14–16] It can also enable

Department of Aeronautics and Astronautics, University of Washington, Seattle, WA, USA

Corresponding author:
Federico Gasco, Department of Aeronautics and Astronautics, University of Washington, Seattle, WA, 98195-2400, USA.
Email: gasco@uw.edu

the simultaneous implementation of electric energy storage and load-bearing capabilities through engineered composite electrodes comprising electrochemically active particles or fibers bound by a structural matrix with electrically conductive filler. Last, nanoscale technology allows better accommodation of the cycling strain induced by Li-ion insertion and removal. Currently, this cyclic strain causes low durability and capacity fading during operation of conventional bulk material electrodes, in particular when silicon is used as anode material for high specific capacity.[17–19]

The low TFB thickness, typically less than 300 μm, facilitates integration within thin sections, but it implies that a significant weight fraction is constituted by the packaging layers. In the proposed configuration, the battery packaging consists of a substrate, which provides mechanical support to the battery manufacturing process, and a sealant, which ensures electrical insulation and sealing of the highly reactive cell components (Figures 1 and 2). The high weight fraction of passive

components, such as the packaging, is a deterrent for most large-scale applications of TFBs, which are instead typically employed as micro power sources for memory chips, microelectromechanical systems (MEMSs) and medical implantable devices. However, if the packaging is by design of an active load-bearing element instead of passive battery mass, this technology becomes an appealing multifunctional system for electric propelled air vehicles. Low-power airborne applications, such as localized power sources for structural health monitoring systems or for fly-by-feel distributed sensing materials, would also benefit from TFBs integrated in the airframe, without requiring a load-bearing battery design.

The manufacturability and functionality of TFBs integrated within structural composite laminates have to be proven in terms of physiochemical compatibility of TFB materials with the composite curing environment, durability of the electrodes, laminate structural integrity and TFB packaging integrity under applied loads. Mechanical tests conducted on a commercially available TFB by Pereira et al.[11] show that the battery is capable of withstanding uniaxial transverse (out-of-plane) pressure up to 830 kPa without any detrimental effects on the electric functionality, thereby indicating that the TFB is compatible with the autoclave curing pressure of epoxy-based composite materials. The same TFB type has been successfully embedded in a carbon/epoxy composite laminate cured at 121°C. TFB failure has been documented for a 177°C cure,[12] giving evidence that the processing temperature is an influential parameter for battery survivability. The ability to tolerate exposure to curing temperatures, which range from 121°C to 177°C, in a quiescent status (e.g. with no electric current flow) is fully covered neither by scientific literature nor by commercial electronics standards. On the other hand, the
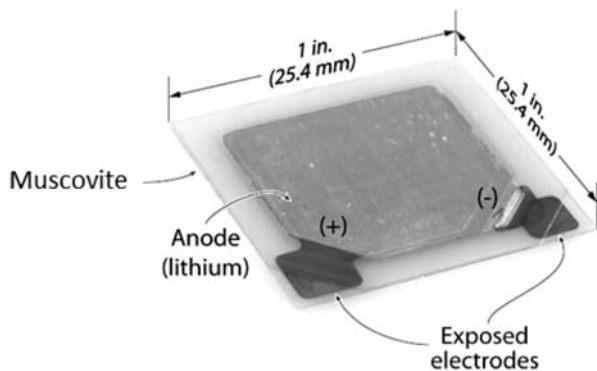

Figure 1. Perspective photo of all-solid-state thin film Li-ion battery with dimensions. Manufactured by Front Edge Technology Inc.
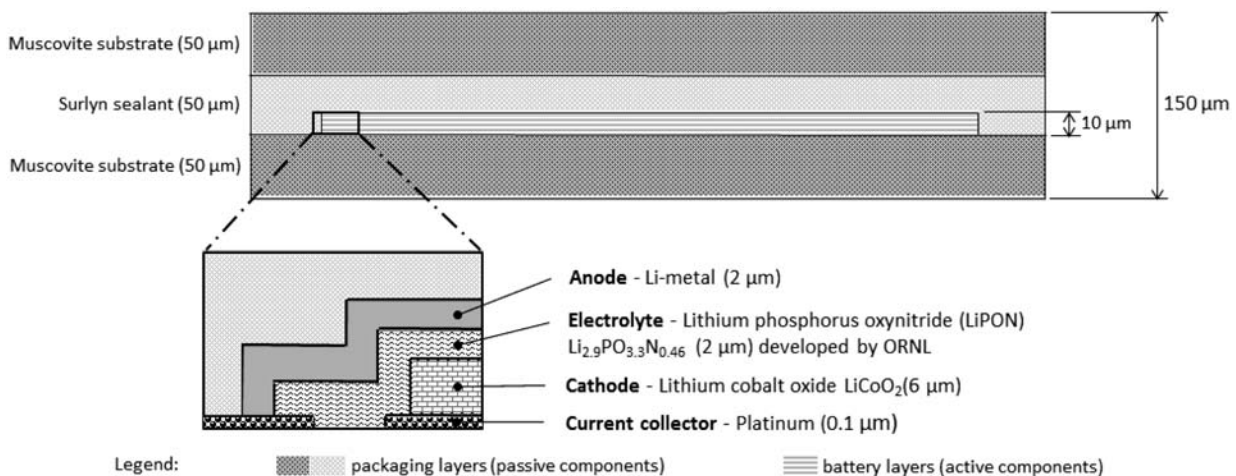

Figure 2. Thin film Li-ion battery cross-sectional schematic.

ability to operate from $-55°C$ to $100°C$ has been extensively investigated because of the relevant commercial applications. High-temperature characterization of TFB with the same chemistry of the batteries tested in the present study has been performed under charge/discharge cycling (e.g. not in a quiescent status) and permanent capacity reduction has been detected at $80°C$.[20] In the study by Van Sluytman et al.,[21] cycling at $100°C$ and $150°C$ causes permanent capacity reduction associated with a decrease in the grain dimension of the lithium cobalt oxide ($LiCoO_2$) cathode, whereas the processing in a quiescent status does not lead to battery capacity loss. The effect of the state of charge, however, has not been investigated. The increasing detrimental effect of temperature exposure at an increasing state of charge[22] up to thermal runaway[23] has been studied only for conventional 18650 Li-ion cells, not for TFBs.

The objective of this study is to experimentally assess the limits of processability and identify the failure types of the current solid-state thin film battery materials within composite curing temperatures and pressures and a liquid resin environment, in order to enable the manufacturing of composite laminates with embedded or externally bonded TFBs. The research covers the $121°C$ to $199°C$ processing temperature range of batteries in a quiescent status at two states of charge, corresponding to the higher and lower limit of the operating charge level.

Methodology

Solid-state thin film Li-ion battery

The TFBs utilized in this research are manufactured by Front Edge Technology under license from the Oak Ridge National Laboratory (ORNL) (Figure 1). The same batteries have been utilized by Pereira et al.[10–13] The cathode material is $LiCoO_2$, the anode is Li metal and the solid-state ceramic electrolyte is lithium phosphorus oxynitride ($Li_{2.9}PO_{3.3}N_{0.46}$), also known as LiPON.[24] This battery chemistry has been electrically characterized in the study by Bates et al.[25] This electrochemical cell generates an electric current outside the cell and a Li-ion flow inside the cell through the simultaneous oxidation reaction of the Li metal contained in the anode and the reduction reaction of the Li ions that occurs at the cathode. This process is called battery discharge. The chemical reactions and corresponding electronic and ionic flow are reversed if an opposed external electric potential is applied to the cell. This process is called battery charge. During discharging, Li ions are extracted by the anode and intercalated at the cathode. Upon charging, Li ions are released by the cathode and plated at the anode.

Unlike conventional batteries, which require a Li intercalation compound as anode material to achieve the required electronic and ionic conductivity, the improved electrochemical kinetics of the thin film structure allows to utilize a metallic Li anode, resulting in higher specific capacity and lower redox potential. These characteristics allow to minimize the anode thickness and to maximize the cell voltage, respectively. $LiCoO_2$ has the highest electronic conductivity and one of the highest specific capacities among the cathode materials that are technology ready. For these reasons it is one of the most popular cathode materials for conventional batteries and the most popular cathode material among commercially available TFBs. LiPON is currently the solid-state electrolyte with the highest ionic conductivity that can be manufactured into thin films. The chemistry of this cell is representative of the commercial state-of-the-art of TFBs, and the electrochemical characterization reported hereinafter enables its use in multifunctional composite structures and can be regarded as a baseline performance for the next generation of nanostructured TFB materials that are not technology ready yet.

The active components are encased by two muscovite substrates bound by a thermoplastic layer of Surlyn sealant, leading to a total thickness of $150\,\mu m$ (Figure 2). Critical temperature thresholds for the TFB materials are summarized in Table 1.

The electrochemically active components of the battery are grown by physical vapor deposition (PVD) performed in situ on the muscovite substrate. The cathode is fabricated through radio frequency (RF) magnetron sputtering and annealing at a high temperature (typically $700°C$) to obtain a crystalline microstructure with large grains and uniform preferred crystalline orientation to maximize ionic conductivity.[26] The muscovite

Table 1. Relevant temperature thresholds for TFB components.

Component	Material	Temperature	Property
Sealant	Surlyn	$98°C$	Melting point
Anode	Lithium	$181°C$	Melting point
Electrolyte	$Li_{2.9}PO_{3.3}N_{0.46}$ (LiPON)	$300°C$	Maximum operating temperature[a]
Cathode	$LiCO_2$	$700°C$	Annealing temperature[b]
Substrate	Muscovite	$700°C$	Calcination temperature
Current collector	Platinum	$1768°C$	Melting point

[a]Yu X., et al. *J Electrochem Soc* 2000; 147(2): 517.
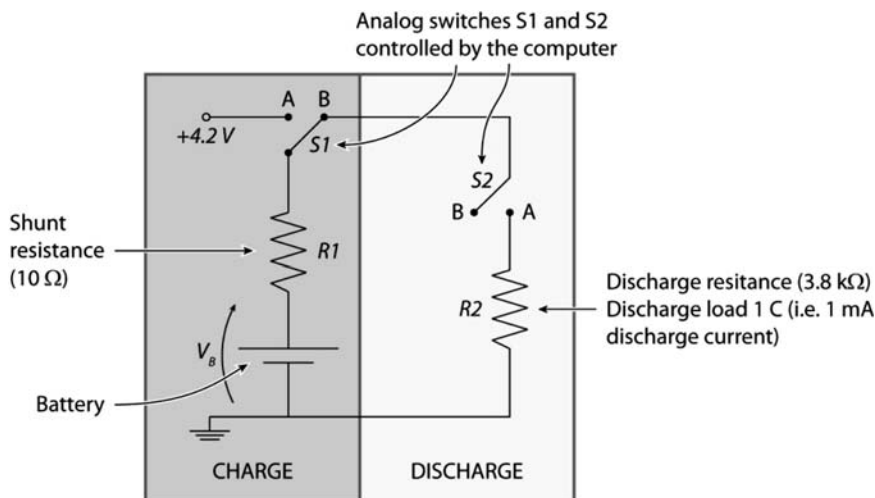[b]Bates JB, et al. *J Electrochem Soc* 2000; 147: 59.

Figure 3. Schematic of the circuit used to test the battery's survivability by monitoring charge and discharge performance before and after thermal processing.

substrate ensures dimensional stability during the annealing process, preventing cathode cracking or disbonding due to thermal stresses. The patented process is described in the study by Krasnov et al.[27] The electrolyte is deposited by RF magnetron sputtering in N_2 atmosphere[28] according to the ORNL process.[24] The Li anode is deposited by thermal evaporation.[25] These materials are highly reactive. Li metal reacts with N_2[24] and O_2[25], while all of the three active component materials react with H_2O.[29] Therefore, the TFB has to be hermetically sealed. A permanent failure of the sealant during manufacturing or operation leads to the failure of the battery by compromising the ability of the electrochemical cell to store energy. The electrical capacity loss that occurs after the failure of the sealant can be almost instantaneous or the capacity can fade progressively, depending on the flow rate of contaminants entering the battery.

The battery is a 25.4 mm^2 with a nominal voltage of 4.2 V, and a nominal capacity of 1 mAh. In order to calculate the actual energy density, the energy delivered by one battery during a full discharge has been measured according to the method described in the next section. The active components of the battery have been separated from the substrate and sealant, and weighed with a Mettler Toledo XS64 analytical balance. The active mass, given by the sum of cathode, electrolyte, anode and current collectors, is 0.0113 g, which leads to an energy density of 353 Wh/kg. The energy density calculated with respect to the total TFB mass is 22 Wh/kg.

Experimental approach

Battery survivability is monitored through discharge and charge cycling prior to and following a thermal
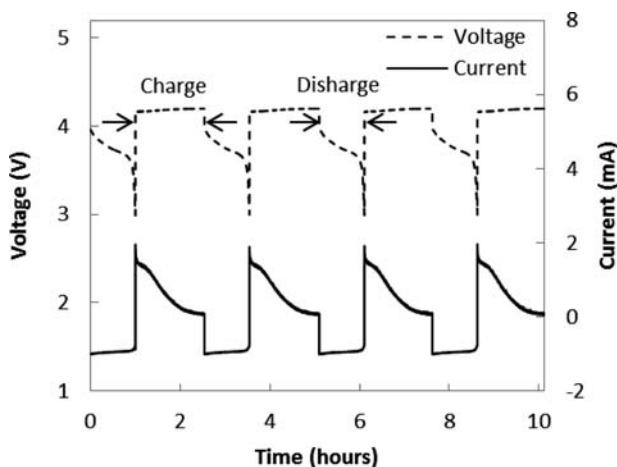

Figure 4. Description of the four discharge and charge cycles for the survivability test.

processing test. The same survivability check is repeated 2 months following the treatment to assess the survivability after aging. An automated circuit board featuring a charge–discharge electronic circuit (Figure 3) is connected to a National Instruments BNC-2120 connector and controlled via a LabView program. Current and voltage readings are collected every 3 s. The discharging occurs under a constant 3.8-kΩ resistive load, which leads to an average discharge current of approximately 1 mA (Figure 4), corresponding to a discharge rate of 1 C. The TFB is considered fully discharged when the voltage reaches 3 V. Immediately following a discharge, charging is performed at a constant voltage of 4.2 V, applied by a Hewlett-Packard 6632A System DC Power Supply. A shunt resistance of 10 Ω is utilized to measure
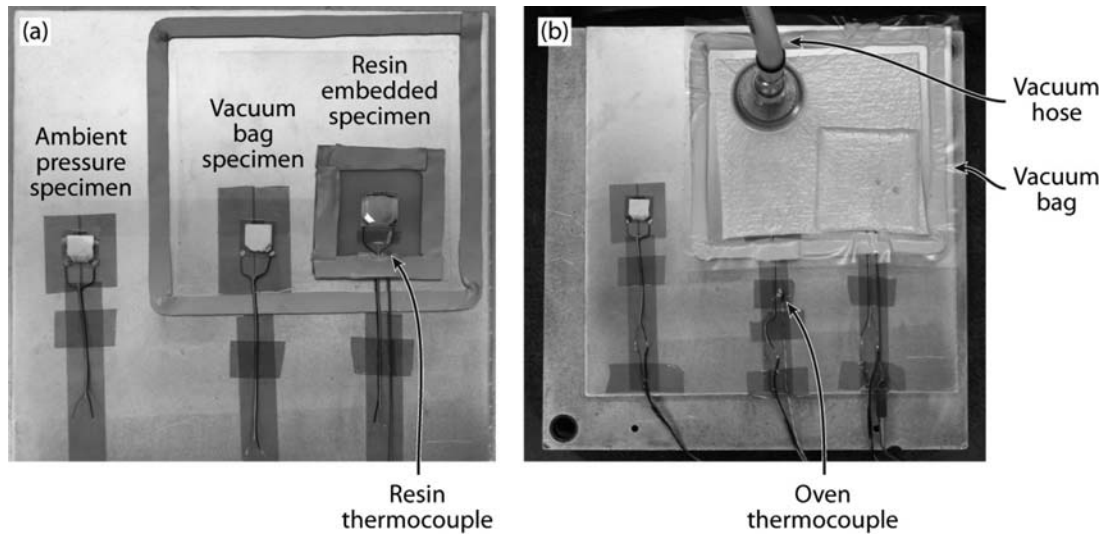
Figure 5. Simultaneous thermal treatment of batteries under ambient pressure, in a vacuum bag and embedded in a neat resin pool. (a) Location of batteries before addition of (b) the vacuum bag.

the current. The battery is considered fully charged when the current drops below 50 μA. For each battery, five charge–discharge cycles are performed; the first is used to condition the battery and the following four provide the average discharge capacity (Figure 4). The capacity is obtained by numerical integration of the discharge current, as a function of time, over a discharge cycle.

In order to assess the limits of processability, the TFBs are subjected to pressure, temperature and a liquid resin environment that is representative of composite curing cycles. The batteries are exposed to a 1-hour isothermal hold at a given temperature, 121°C, 149°C, 177°C or 199°C. For each temperature, one battery is tested at ambient pressure, a second is placed under a 28-mm Hg vacuum and a third is embedded in a $50.8 \times 50.8 \times 3.8$ mm^3 pool of Fiberlay Pro Glas 1300 series neat epoxy resin under a 28-mm Hg vacuum. The vacuum is created within a flexible nylon bag in order to apply a hydrostatic pressure to the resin (Figure 5).

A sample of batteries is thermally processed at 121°C in a fully charged state and in a partially charged state to determine if the state of charge affects battery survivability. In order to avoid over-discharging of the batteries, as recommended by Front Edge, the partial state of charge is achieved by discharging to $3.9 V_{OC}$ (open circuit voltage) prior to thermal processing. Based on these preliminary results, which give evidence of the detrimental effect of the full-charge status on the TFB capacity retention, only partially charged TFBs are tested at higher temperatures.

Temperatures are recorded by a LabView program, which monitors the oven temperature and the resin temperature from two independent thermocouples via a National Instrument USB-6210 multifunctional data acquisition (DAQ) module. A Despatch LAC bench-top ventilation oven heats the specimens at a rate of 5°C/min from room temperature to the test temperature. The test is conducted under an electrical load of 108 kΩ (R3) to facilitate battery failure detection. The current drained from the batteries is small enough to consider the state of charge constant throughout the test. Voltages and currents are recorded by the DAQ and LabView program with a frequency of one measurement every 3 s (Figure 6).

A total of 18 batteries have been subjected to the thermal processing test. Based on the results, a cure cycle has been designed and validated through embedding tests in glass fiber/epoxy (GFRP) and carbon fiber/epoxy (CFRP) composite laminates. The TFB is embedded at the midplane of the laminate (Figure 7). Two slits in the top layers of the laminates allow for the flat flexible cables (FFCs), Nicomatic 254PW01E6095 polyester-coated single copper conductor, to exit the laminate. FFCs are 0.25 mm thick and 5.12 mm wide, and they are rated for operation up to 150°C for short durations and to 100°C for continuous use. They are connected to the TFB electrodes using MG Chemicals silver conductive epoxy 8331-14 G. The glass/epoxy composite material utilized is Toray AGATE prepreg glass fiber FGF7781/2510, 8 harness satin weave fabric. The 4-ply laminate is cured at 132°C and 520 kPa for 2 h through heated press molding. The laminate stacking sequence is [0,90]$_4$. The battery is located at the panel mid-span (Figure 8). A second embedding test is performed using Toray AGATE prepreg carbon fiber tape T700/2510 with stacking
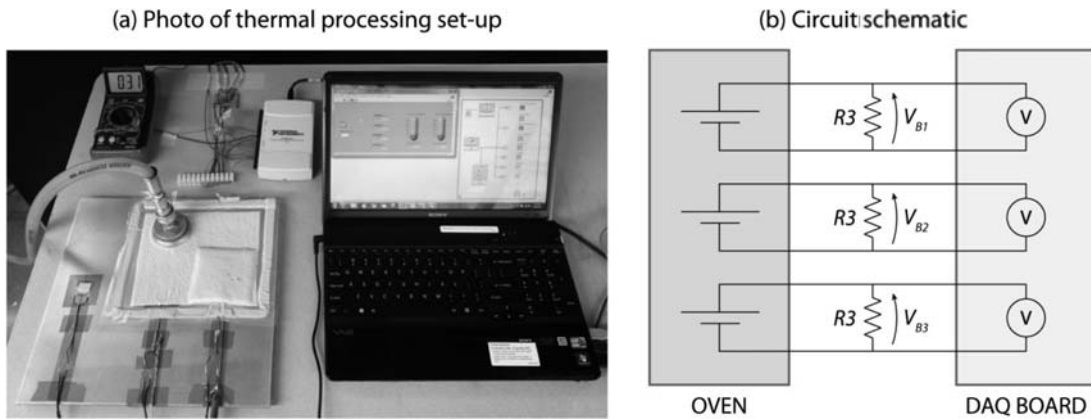
Figure 6. Battery and thermocouple voltages are recorded by a LabView program via the DAQ board during thermal testing under electrical load. (a) Set-up before the specimen tray is placed in the oven. (b) Circuit schematic including thin film Li-ion battery inside the oven and resistive load (R3) outside the oven.
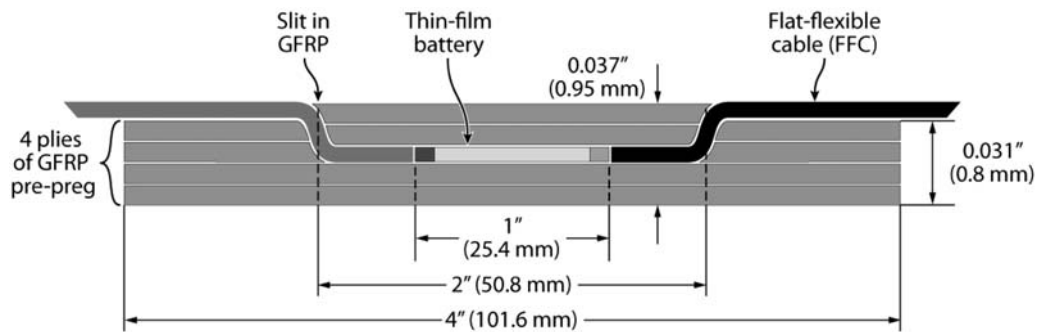DAQ: data acquisition.

Figure 7. Cross-sectional schematic of a thin film battery embedded at the mid-plane of a four-ply glass fiber reinforced polymer laminate. Two slits in the top two layers allow for the flat flexible cable to exit the panel.
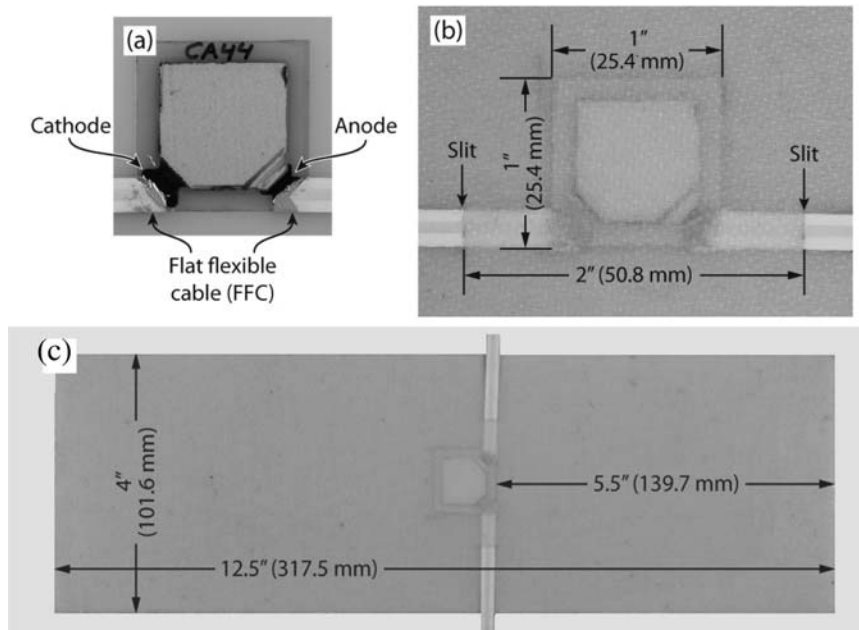

Figure 8. Photos of a battery (a) before and (b) after embedding within a glass fiber reinforced polymer laminate; (c) panel with the embedded battery.
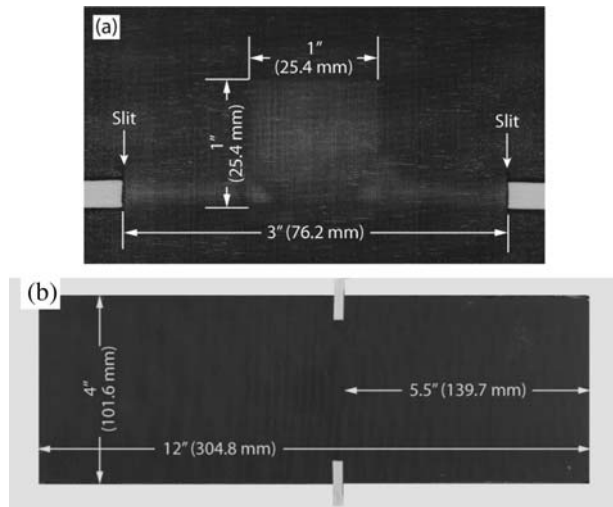
Figure 9. Photos of a carbon fiber reinforced polymer panel with embedded thin film Li-ion battery showing (a) a close-up of the panel at battery location and (b) the whole panel.

sequence $[0/90]_{2s}$ (Figure 9). The same fabrication process is adopted with the addition of a localized application of silicone conformal coating MG Chemicals 422-55 on the exposed battery leads to insulate the connections. Attempts of embedding the TFB without insulated connections have failed due to electrical shorts caused by the CFRP.

Results

Typical temperature and voltage profiles for the thermal processing test are shown in Figure 10. The battery voltage, regardless of the processing environment, decreases with increasing ambient temperature and recovers its initial value when the battery is brought back to room temperature at the end of the 1-hour-long isothermal phase. During temperature ramp-up, the resin temperature shows a spike due to the exothermic reaction associated with the resin cross-linking. The maximum difference between resin and oven temperature during cross-linking never exceeds 15°C, and the peak temperature never exceeds the isothermal hold temperature. The voltage of the battery embedded in neat resin shows a negative spike, which corresponds to the beginning of the exothermic event. This voltage drop, which lasts 3–9 s, has been observed for all of the TFBs processed in the neat resin without having any detrimental effect on the survivability of the battery. While the reason for the voltage drop is unknown, the fact that it has occurred during embedment within Fiberlay Pro Glas 1300 neat epoxy resin, but it has not occurred during the embedment in the Toray 2510 and Cytec 977-3 prepreg resin systems, suggests that possible causes should be dependent on the resin chemical
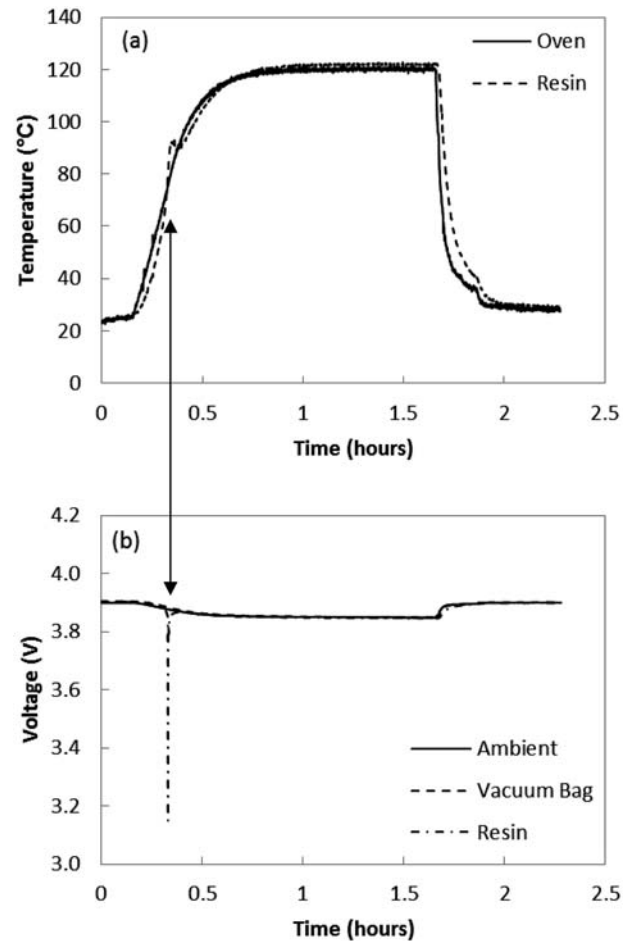

Figure 10. (a) Typical temperature cycle for thin film Li-ion battery thermal processing test. The temperature profile for the oven and neat resin is shown for a 1-hour isotherm at 121°C. (b) Voltages of the three batteries shown in Figure 5 undertaking the thermal treatment. A voltage drop of the battery embedded within the resin coincides with heat generation by the resin due to exothermal cross-linking reaction.

composition or on the amount of resin undertaking exothermic reaction.

Thermal testing at 121°C of fully charged batteries leads to an average capacity reduction of 9%, as summarized in Table 2. The capacity reduction is proportional to a reduction in discharge time, whereas the cell voltage and power are unchanged (Figure 11). On the other hand, if the TFBs are partially discharged to 3.9 V before being tested, they withstand thermal processing up to 149°C without any detrimental effects on their electric performance. The detailed summary of the results (Tables 3 and 4) shows that the short-term and long-term capacities after thermal processing remain within ±3% of the baseline capacity measured before the test. The capacity variation is associated with a slight offset of the discharge current and voltage profiles (Figure 12). Neither the liquid resin nor the

Table 2. Capacity retention of batteries undergoing a 1-hour isothermal hold at 121°C in either a fully charged state or partially charged to 3.9 V_{OC} (open circuit voltage).

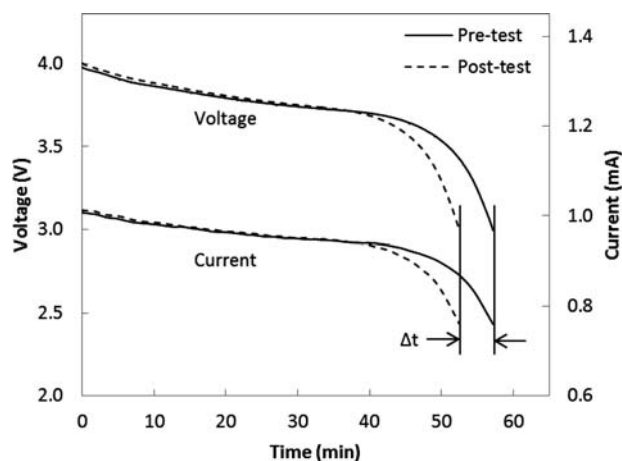|	Fully charged		Partially charged	
	Capacity retention (%)	Survival rate	Capacity retention (%)	Survival rate
Ambient	94	1/1	102	1/1
Vacuum bag	95	1/1	102	1/1
Neat resin	84	1/1	102	1/1

Figure 11. A discharge profile from the survivability test for a fully charged battery subjected to a 1-hour isotherm at 121°C under ambient pressure. The decrease in the discharging time is proportional to the 6% decrease in capacity retention after processing (see Table 2).

Table 3. Survival rate of partially charged batteries subjected to temperatures, pressures and liquid resin environment typical of composite manufacturing.

	Isothermal temperature			
	121°C	149°C	177°C	199°C
Ambient	1/1	1/1	1/2	0/1
Vacuum bag	1/1	1/1	(2)/2	0/1
Neat resin	1/1	1/1	0/2	0/1

Parentheses indicate failure after 2 months of aging.

vacuum bag environment seems to have an effect at this processing temperature. All the batteries tested at 177°C, either at ambient pressure or in the vacuum bag, are affected by partial or total capacity loss (Tables 3 and 4) associated with a decreased discharge time and a negative translation of the current and

Table 4. Average discharge capacity retention of survived batteries from Table 3.

	Isothermal temperature			
	121°C	149°C	177°C	199°C
Ambient	102% (100%)	100% (100%)	76% (70%)	0%
Vacuum bag	102% (100%)	103% (100%)	87% (0%)	0%
Neat resin	102% (100%)	98% (98%)	0%	0%

Values in parenthesis are measured 2 months after test.

Table 5. Survival of partially discharged batteries embedded in either a GFRP or a CFRP laminate cured at 132°C and 520 kPa.

	Capacity retention (%)	Survival rate
CFRP	103	1/1
GFRP	102	1/1

CFRP: carbon fiber reinforced polymer; GFRP: glass fiber reinforced polymer.
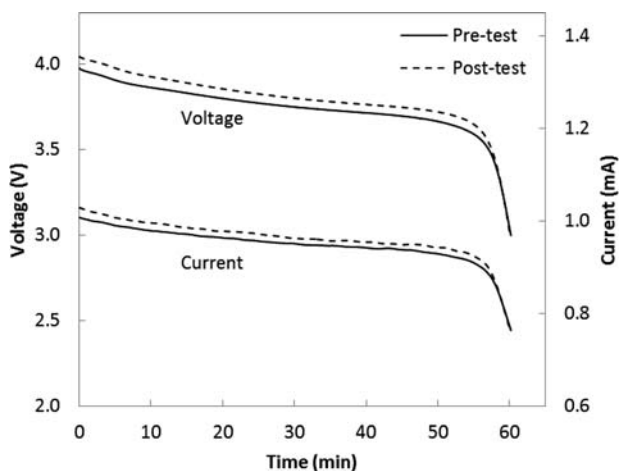

Figure 12. A discharge profile from the survivability test for a partially charged battery subjected to a 1-hour isotherm at 121°C under ambient pressure. The battery had 102% capacity retention after processing (see Table 2).

voltage discharge profile (Figures 13 and 14). The batteries embedded in neat resin at 177°C, as well as all the ones processed at 199°C, failed during testing.

Three distinct types of failures have been recognized and characterized based on optical microscopy at the anode side and capacity retention (Figure 15(a) to (d)). Type I failure (Figure 15(b,bb)) is observed as a localized gray spot on the Li anode with a complete loss of grain boundaries. Front Edge Technology attributes these observations to electronic failures consisting of
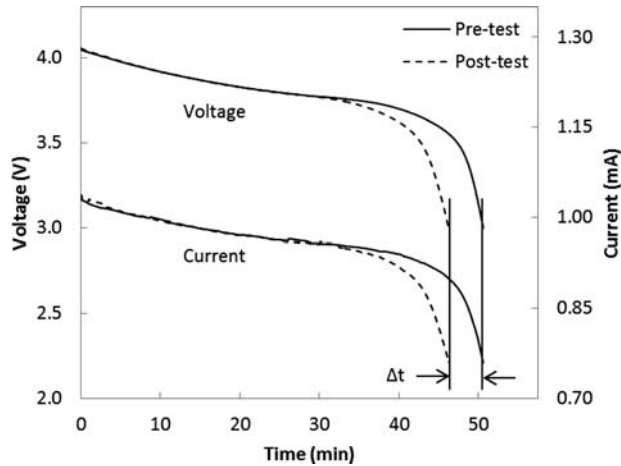
Figure 13. A discharge profile for a partially charged battery subjected to a 1-hour isotherm at 177°C under vacuum. The battery had 91% capacity retention after processing, ultimately failing with aging (see Table 3).
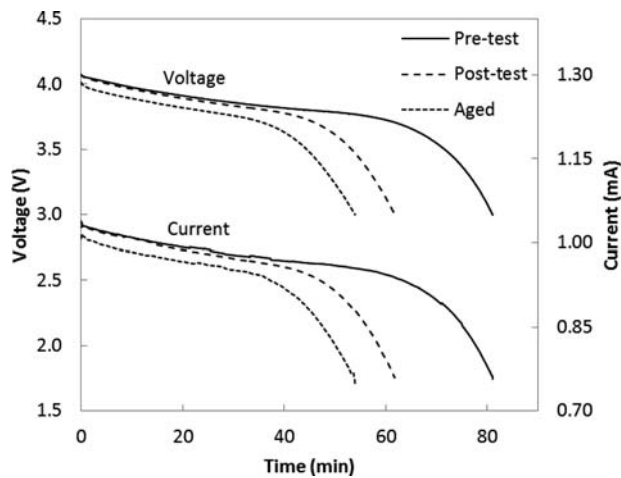

Figure 14. A discharge profile from the survivability test for a partially charged battery subjected to a 1-hour isotherm at 177°C under ambient pressure. The battery had 76% capacity retention after processing, reducing to 70% with 2 months of aging.

a local breakdown of the electrolyte. The gray spot is always associated with bubbling of the overlaying Surlyn sealant layer at the failure location. This failure occurs in batteries processed at ambient pressure or within the vacuum bag. The affected batteries are operational, but with reduced capacity. Type II failure produces a neutral gray discoloration, which extends from the edges of the active components (Figure 15(c,cc)). The micrographs reveal dark patches scattered across the anode. It is believed that this failure is caused by the reaction of the Li anode with contaminants diffusing through the Surlyn sealant and entering into the battery.

The appearance of Type II failure always leads to total capacity loss. This failure is observed after thermal processing of batteries embedded in neat resin, or in aged batteries previously processed at 177°C. The Type III failure shown in Figure 15(d,dd) has occurred for all of the batteries tested at 199°C. The failure occurs above 177°C during the temperature ramp-up, leading to a sudden loss of voltage and battery failure. This failure is due to Li melting (MP 181°C) and the TFB becomes black at the anode side, occasionally showing gray spots that are probably Type I failures formed prior to the melting of the anode.

The battery shown in Figure 16 is affected by Type I failure and the associated capacity reduction caused by processing at 177°C in the vacuum bag. With aging, however, this battery completely fails by Type II failure. This indicates that the Type II failure is time-dependent. A similar result is observed when the battery seal is artificially compromised under ambient conditions. Hence, the low-temperature thermoplastic sealant (MP 98°C) seems to be the limiting factor for survivability from a manufacturing standpoint.

Further examination of treated batteries reveals that sealant bubbling and flowing affects TFBs tested at temperatures as low as 121°C. This leads to the formation of a disbonded front along the edges of the active components (Figure 17(b)) and over the leads (Figure 17(c)). For the TFBs processed under vacuum bag, the sealant is squeezed out of the battery edges (Figure 17(d)). However, the functionality of these batteries, as tested for short- and long-term survivability, is not affected. Further screening conducted on as-received batteries revealed that some have long strands of bubbles along the edges of the active components. The bubbles are suspected of diffusing within the sealant layer when the processing temperature leads to melting of the Surlyn. Depending on the concentration of bubbles and the viscosity of the sealant, access paths to the active components could propagate through the sealant itself.

Based on these findings, successful embedding tests with full capacity retention (Table 5) are performed by co-bonding the TFB within a composite laminate through press molding of prepreg materials at 132°C and 517 kPa, with a cure time of 2 h (Figures 7 to 9).

Conclusions

This study identified the limits of processability of solid-state thin film Li batteries embedded into composite laminates. Cure temperature is the most influential parameter for battery survivability during composite manufacturing. Successful embedding tests with full-capacity retention have been performed with glass fiber/epoxy and carbon fiber/epoxy cured at 132°C
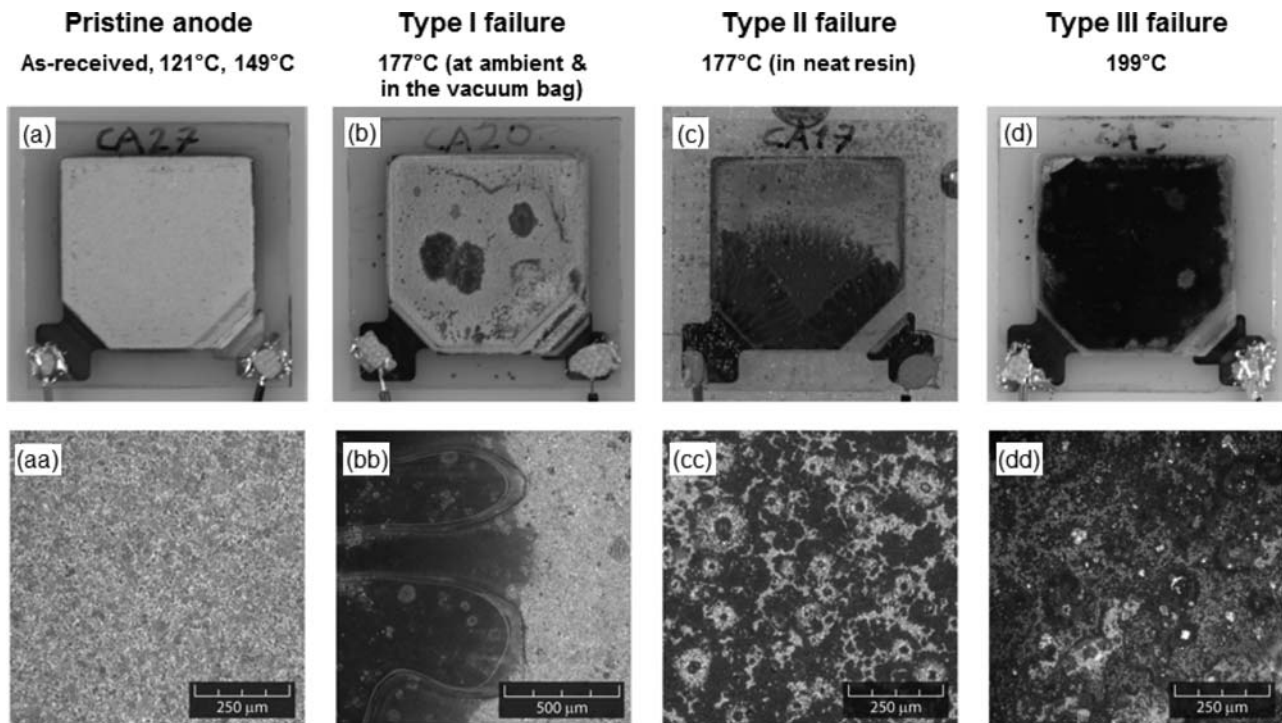
Figure 15. Anode side photos of the three observed types of failures ((b), (c) and (d)) compared to an as-received battery (a). Corresponding dark-field optical micrographs are shown in (aa) through (dd). Type I failure is associated with a local breakdown of the electrolyte and bubbling of the sealant (Surlyn MP of 98°C). Reaction of the anode with contaminants results in a Type II failure. Type III failure occurs above the Li melting temperature (181°C). Type I leads to partial capacity loss; Type II and Type III lead to total capacity loss.
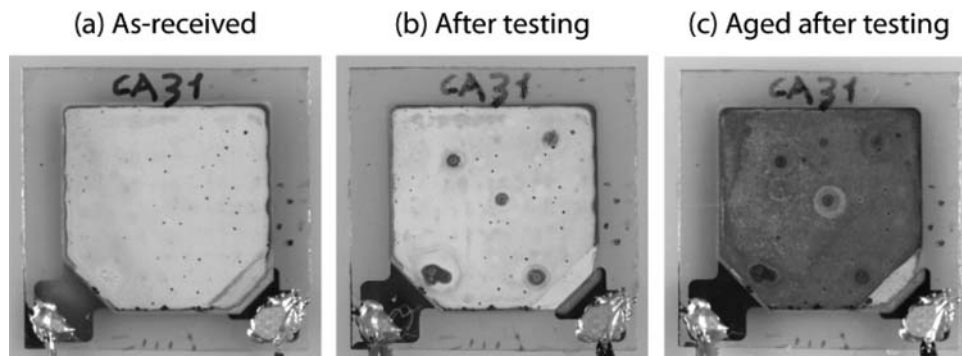

Figure 16. A battery thermally tested at 177°C in the vacuum bag for an hour showing (b) the formation of Type I failures immediately after testing, followed by (c) Type II formations with 2 months of aging. Immediately after testing, the cell exhibited 87% capacity retention; however, it completely failed with aging.

and 517 kPa. With the proper procedure, it is possible to successfully cure the battery inside the laminate up to 149°C. If higher processing temperatures are reached, either locally due to resin exothermic reaction or by design, the battery's electrical performance deteriorates. Battery failures are caused either by the TFB polymeric sealant failure or by the physicochemical degradation of the electrolyte or the Li anode. Ongoing research is focused on the mechanical and electrical characterization of laminates with embedded batteries under applied strain and curvature. The integration of all-solid-state thin film batteries within composite laminates can find
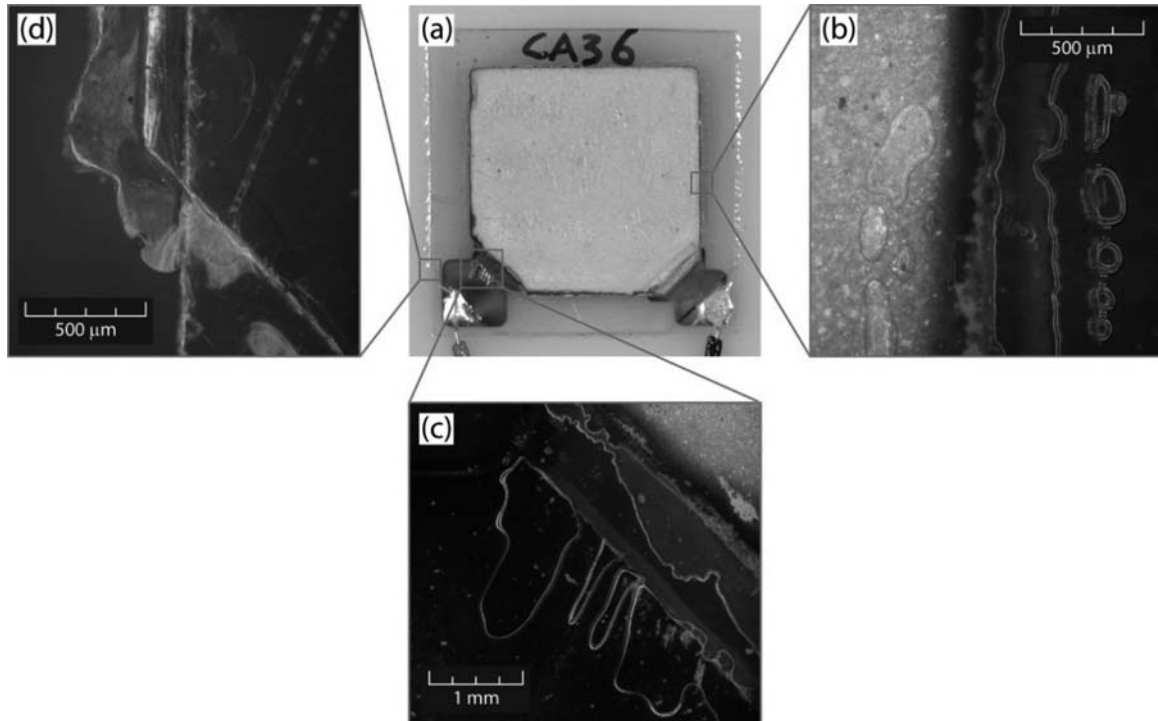
Figure 17. The appearance of bubbles and a disbonded front (b) along the edge of the active components and (c) over the leads after 121°C processing. In some as-received batteries, bubbles are apparent along the edge of the active components. (d) shows the Surlyn that has been squeezed out of between the muscovite layers (exhibiting a slight offset); this is typical of the specimens tested under vacuum bag.
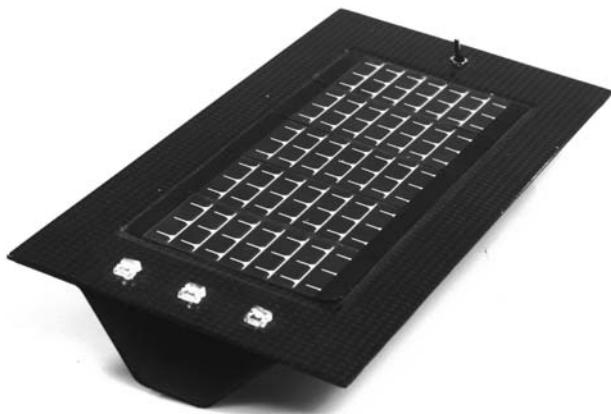

Figure 18. Working prototype of energy self-sufficient carbon fiber reinforced polymer stiffened panel with integrated thin film Li-ion batteries and flexible solar array.

application in commercial and military lightweight multifunctional structures (Figure 18).

Conflict of interest

None declared.

References

1. Thomas JP, Qidwai MA, Matic P, et al. Multifunctional structure-plus-power concepts. In: *Proceedings of 43rd AIAA/ASME/ASCE/AHS/ASC structures, structural dynamics, and materials conference*. Denver, CO, 2002.
2. Thomas JP and Qidwai MA. Mechanical design and performance of composite multifunctional materials. *Acta Mater* 2004; 52: 2155–2164.
3. Thomas JP and Qidwai MA. The design and application of multifunctional structure-battery material systems. *JOM* 2005; 57(3): 18–24.

4. Qidway MA, Baucom JN, Thomas JP, et al. Multifunctional applications of thin film Li polymer battery cells. *Mater Sci Forum* 2005; 492: 157–162.

5. Liu E, Sherman E and Jacobsen A. Design and fabrication of multifunctional structural batteries. *J Power Sources* 2008; 189(1): 646–650.

6. Snyder JF, Carter RH and Wetzel ED. Electrochemical and mechanical behavior in mechanically robust solid polymer electrolytes for use in multifunctional structural batteries. *Chem Mater* 2007; 19(3): 3793–3801.

7. Snyder JF, Wetzel ED and Watson CM. Improving multifunctional behavior in structural electrolytes through copolymerization of structure- and conductivity-promoting monomers. *Polymer* 2009; 50: 4906–4916.

8. Snyder JF, Wong EL and Hubbard CW. Evaluation of commercially available carbon fibers, fabrics and papers for potential use in multifunctional energy storage applications. *J Electrochem Soc* 2009; 156(3): 215–224.

9. Xu C, Ma C and Taya M. Electrolyte for laminated polymer lithium rechargeable battery. Electroactive Polymer Actuators and Devices (EAPAD). *Proc SPIE* 2008; 6927(692714): 1–9.

10. Pereira T, Scaffaro R, Nieh S, et al. The performance of thin-film Li-ion batteries under flexural deflection. *J Micromech Microeng* 2006; 16: 2714–2721.

11. Pereira T, Scaffaro R, Nieh S, et al. Performance of thin-film lithium energy cells under uniaxial pressure. *Adv Eng Mater* 2008; 10(4): 393–399.

12. Pereira T, Scaffaro R, Nieh S, et al. Embedding thin-film lithium energy cells in structural composites. *Compos Sci Technol* 2008; 68(7–8): 1935–1941.

13. Pereira T, Scaffaro R, Nieh S, et al. Energy storage structural composites: a review. *J Compos Mater* 2009; 43(5): 549–560.

14. Liu Y and Taya M. Electrospinning fabrication and electrochemical properties of lithium cobalt nanofibers for lithium battery cathode. Active and Passive Smart Structures and Integrated Systems. *Proc SPIE* 2009; 7288(728806): 1–7.

15. Wang Y and Cao G. Developments in nanostructured cathode materials for high-performance lithium-ion batteries. *Adv Mater* 2008; 20: 2251–2269.

16. Scott ID, Jung YS, Cavanagh AS, et al. Ultrathin coatings on nano-$LiCoO_2$ for Li-ion vehicular applications. *Nano Lett* 2011; 11: 414–418.

17. Chan CK, Peng H, Liu G, et al. High performance lithium battery anodes using silicon nanowires. *Nat Nanotechnol* 2008; 3: 31–35.

18. Trevey JE, Wang J, DeLuca CM, et al. Nanostructured silicon electrodes for solid-state 3-d rechargeable lithium batteries. *Sens Actuat A* 2011; 167: 139–145.

19. Son SB, Trevey JE, Roh H, et al. Microstructure study of electrochemically driven Li_xSi. *Adv Energy Mater* 2011; 1: 1199–1204.

20. Nagasubramanian G and Doughty DH. Electrical characterization of all-solid-state thin film batteries. *J Power Sources* 2004; 136: 395–400.

21. Van Sluytman JS, West WC, Whitacre JF, et al. Cycling-induced degradation of $LiCoO_2$ thin-film cathodes at elevated temperature. *Electrochim Acta* 2006; 51: 3001–3007.

22. Thomas EV, Case HL, Doughty DH, et al. Accelerated power degradation of Li-ion cells. *J Power Sources* 2003; 124: 254–260.

23. Roth EP and Doughty DH. Thermal abuse performance of high-power 18650 Li-ion cells. *J Power Sources* 2003; 128: 308–318.

24. Bates JB, Dudney NJ, Gruzalsky GR, et al. Electrical properties of amorphous lithium electrolyte thin films. *Solid State Ionics* 1992; 53–56: 647–654.

25. Bates JB, Dudney NJ, Neudecker B, et al. Thin film lithium and lithium-ion batteries. *Solid State Ionics* 2000; 135: 33–45.

26. Bates JB, Dudney NJ, Neudecker BJ, et al. Preferred orientation of polycrystalline $LiCoO_2$ films. *J Electrochem Soc* 2000; 147(1): 59–70.

27. Krasnov V, Nieh K and Li J. Thin film battery and manufacturing method. Patent No. 7862927, USA, 2011.

28. Krasnov V, Nieh K, Ting S, et al. Sputter deposition of lithium phosphorous oxynitride material. Patent No. 6863699, USA, 2005.

29. West WC, Whitacre JF, White V, et al. Fabrication and testing of all solid-state microscale lithium batteries for microspacecraft applications. *J Micromech Microeng* 2002; 12: 58–62.